MAE 766 Project #1:
2-D Finite Element Method

by

Kyle Thompson

Revised

Abstract

Finite element methods have a strong theoretical background and can be used to solve the variational formulation of differential equations. Velocity potential can be modeled by Laplace's equation, and solved using the finite element method on unstructured grids. Two cases were run, simulating flow internal flow in a channel with a circular bump and external flow around a cylinder, both 2-dimensional. In both cases the velocity potential and velocity magnitude contours were solved and plotted, and a grid refinement study was performed for the cylinder case. Four increasingly fine grids were solved, and the L2 error norm was computed by comparing the approximate calculated solution with the exact analytic solution. This was used in conjunction with the average mesh spacing to determine the order of accuracy of this implementation of the finite element method.

Introduction

Computational fluid dynamics is centered upon studying and modeling complex fluid flows. While fluid motion is continuous, to simulate this motion the domain space of the fluid must be discretized and solved at set of discrete points. The method of discretizing a continuous dimensional space is centered on two different practices: structured grids and unstructured grids. A structured grid has an ordered number of points, with each points location and cell designation easily determined by that ordering. An unstructured grid, however, has no ordering implicit ordering; therefore, a connectivity matrix must be supplied with the grid point coordinates to determine the corresponding elements associated with each cell. Once a structured or unstructured grid has been generated for a problem, various methods can be used to solve the governing equations and obtain a solution at each point. Finite element methods are one such method, and are based on the variational formulation. This method is versatile, in that it may be used either on structured or unstructured grids, and it has a strong theoretical background.

Method of Solution

For this project, the velocity and velocity potential for two cases were calculated. The first case involved internal flow through a channel with a bump in it. The second case involved external flow around a cylinder. The velocity potential is given by Laplace's Equation:

$$-\Delta\varphi = 0 \tag{1}$$

Where φ is the velocity potential. This can be rewritten as the weak (variational) formulation:

$$\sum_{i=1}^{N}\left\{\int \nabla B_i \cdot \nabla B_j \, d\Omega\right\} * \varphi_i = \int g B_i d\Gamma \tag{2}$$

Where B_i and B_j are the basis function at points i and j, respectively, g is the element face normal vector, and Ω and Γ are the element domain and surface, respectively. The basis function for a 2-D triangle element can be computed as the shape function, given by:

$$B_i = \frac{a_i + b_i + c_i}{D} \qquad i = 1,2,3 \tag{3}$$

$$a_i = y_{i+1} - y_{i+2}$$

$$b_i = -(x_{i+1} - x_{i+2})$$

$$D = a(1) * b(2) - a(2) * b(1)$$

Because the variational formulation only requires the gradients of the basis function, c_i is trivial, and need not be calculated. D is twice the area of a cell.

By computing the basis function at each point, and accounting for multiple elements with the same point, the variational formulation reduces to:

$$A\varphi = b \tag{4}$$

Where A is the stiffness matrix composed of the calculated basis functions for all points, b is the load vector containing the Neumann boundary conditions of uniform inflow of velocity in the x direction, equal to 1 m/s, and φ is the solution vector. In order to obtain a unique solution, a Dirchlet boundary condition must be imposed. For the channel case, this was arbitrarily chosen, but for the cylinder case, the analytic solution was computed at one of the boundary points and imposed, so the solution obtained would match the analytic solution. This was done by multiplying a boundary point on the right hand side of the equation by an arbitrary large number and multiplying the corresponding load vector entry by that same number times the exact solution at that boundary point. A Point Jacobi scheme was then used to solve equation (4).

With the solution vector for the velocity potential obtained, the velocity may be obtain at each cell by:

$$V_i = \sum_{j=1}^{3} \frac{\partial B_j}{\partial x_i} * \varphi_j \tag{5}$$

With the velocity calculated at each cell, it may then be interpolated to each point by an area-weighted average.

In order to determine the order of accuracy of the finite element method, a grid refinement study was conducted for the cylinder case. Four increasingly fine grids were solved and compared to the exact analytic solution, so that the order of accuracy could be determined. Assuming a relationship between the error and the mesh spacing, we can derive the following:

$$\varepsilon = Ch^{\alpha}$$

$$\log \mathcal{E} = \log C + \alpha * \log h \tag{6}$$

Where $\mathcal{E}$ is the L2 error norm, C is an arbitrary constant, h is the mesh spacing, and α is the slope, which is the order of accuracy.

Results

The grid for the channel flow and the finest mesh for the cylinder flow are show in figure 1, to aid in understanding the grid geometry.

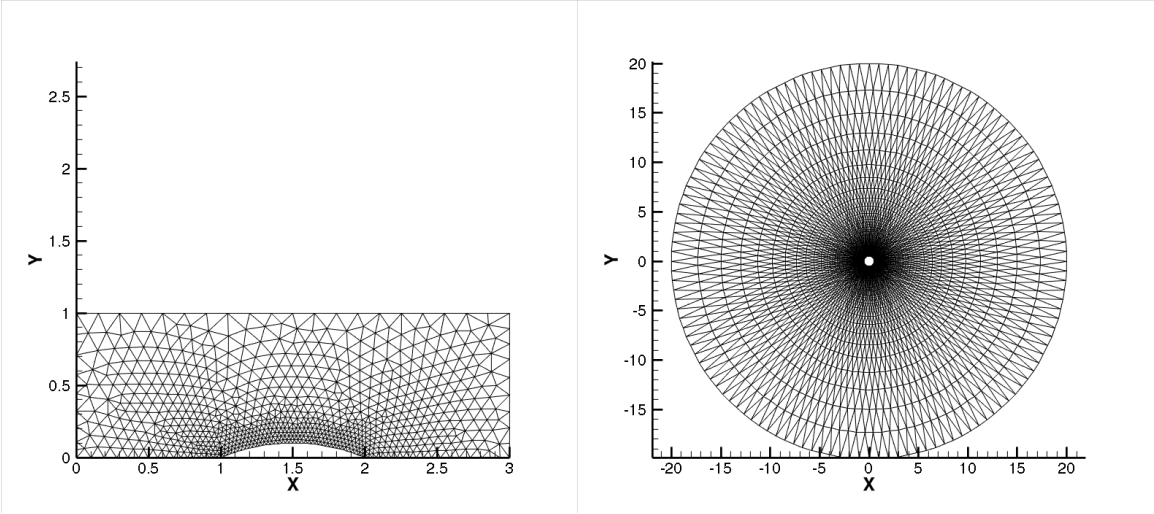

Figure 1. Channel Grid (Left) and Finest Cylinder Grid (Right)

The channel flow the velocity potential and velocity magnitude is shown in figure 2:

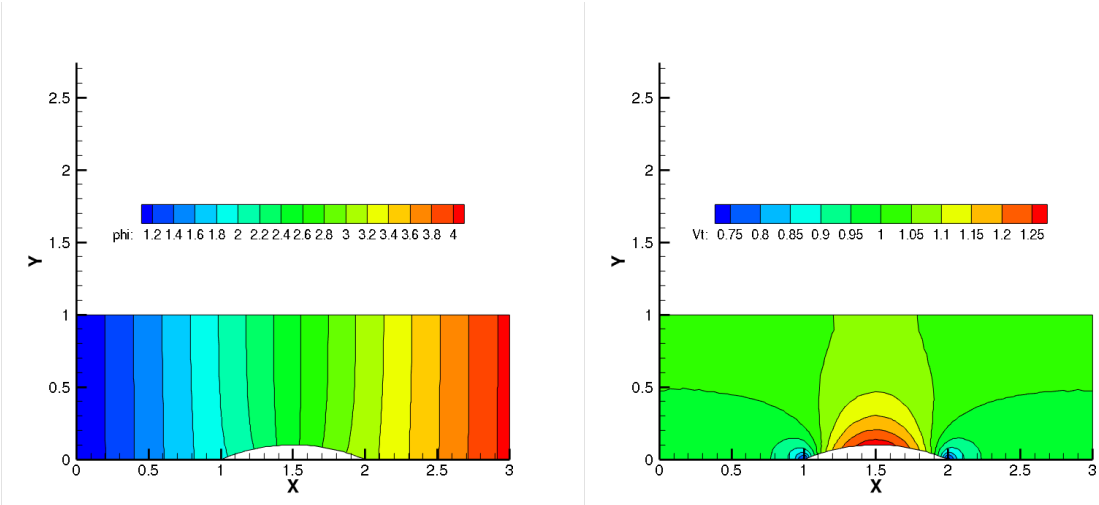

Figure 2. Channel Velocity Potential (Left) and Velocity Magnitude (Right)

The contours clearly show the expected acceleration of the flow as it travels over the circular bump in the channel, as you might see in a Venturi tube. It should be noted that SI units were used; thus, the dimensions for velocity potential are m^2/s and the dimensions for velocity are m/s, for all cases.

Figure 3 shows the streamlines on the upper and lower walls of the channel superimposed over the velocity magnitude contours:

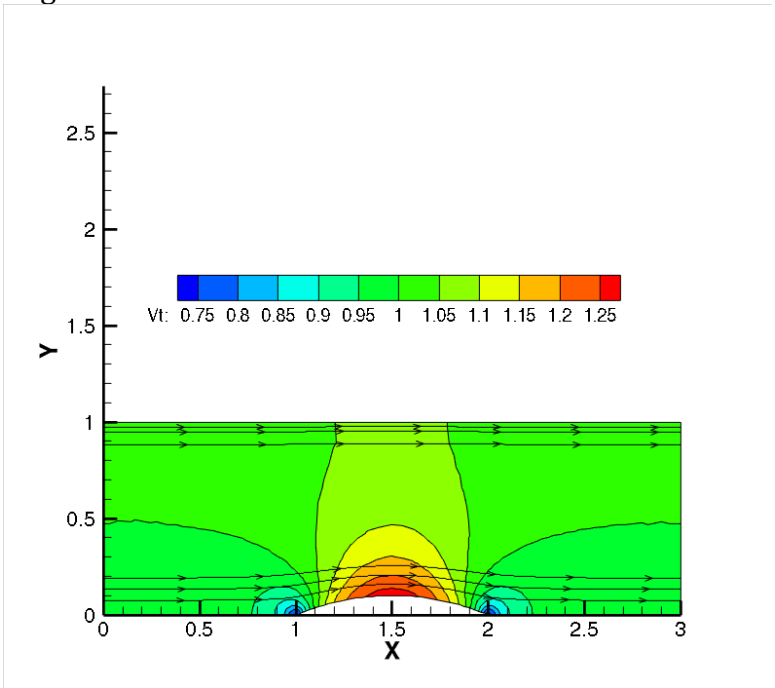

Figure 3. Velocity Stream Traces over the Velocity Magnitude Contours

These also agree with the expected affect of the circular bump, with the flow smoothly moving around the bump, all the way up to the upper wall. Figure 4 shows the surface velocity at the upper and lower surface of the channel:

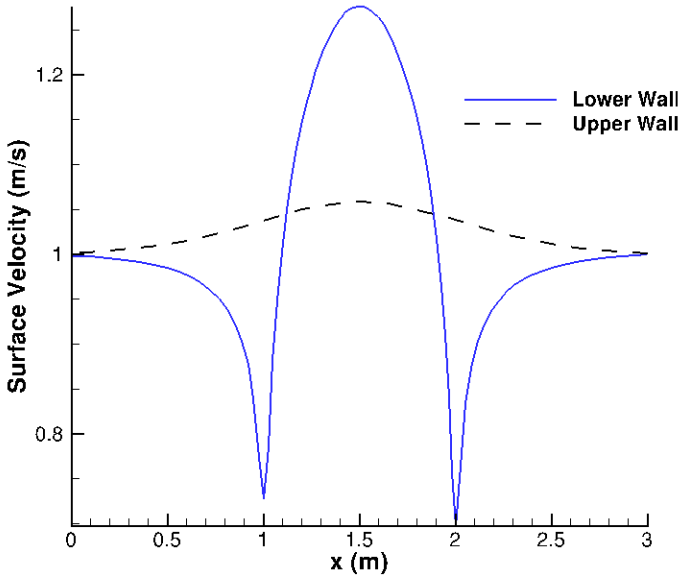

Figure 4. Surface Velocity in the Channel

The difference in magnitude between the top and bottom surfaces is expected, since there is only a bump on the bottom of the channel. The sharp drop in velocity before and after the circular bump is peculiar, and could be due to something of "mini-stagnation point" where the flow accelerates afterwards similar to a Venturi tube and then loses velocity with the area increase.

Figure 4 shows the cylinder flow potential and velocity magnitude contours:

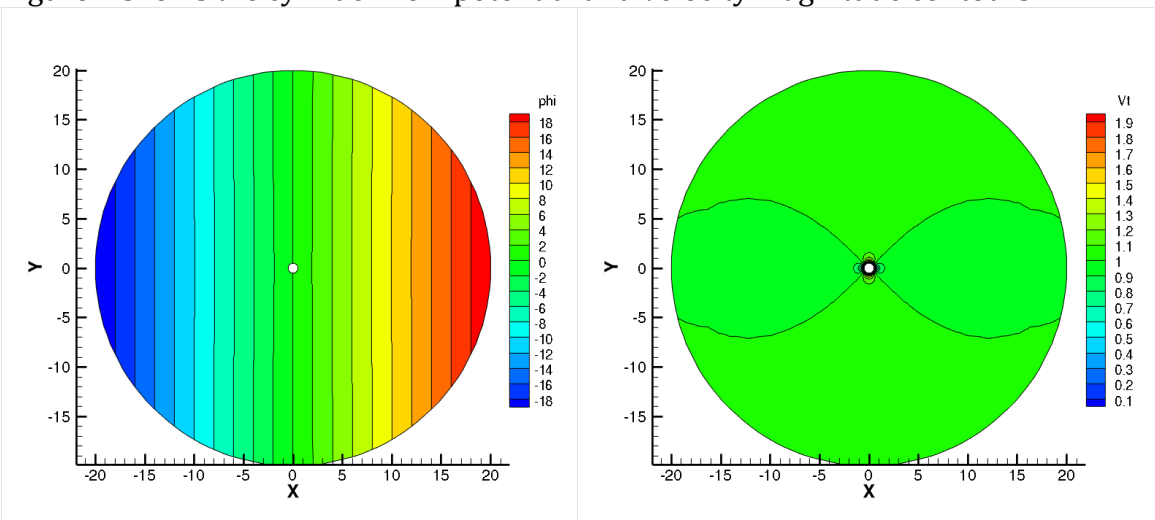

Figure 5. Cylinder Velocity Potential (Left) and Velocity Magnitude (Right) Contours

These contours clearly show that the velocity potential isolines are symmetric and perpendicular to the cylinder, as expected. The velocity magnitude contours also agree with expectation that the far field flow is nearly uniform, while the velocity near the surface is symmetric, but not uniform.

Figure 5 shows the streamlines near the cylinder surface, superimposed over the velocity magnitude contours:

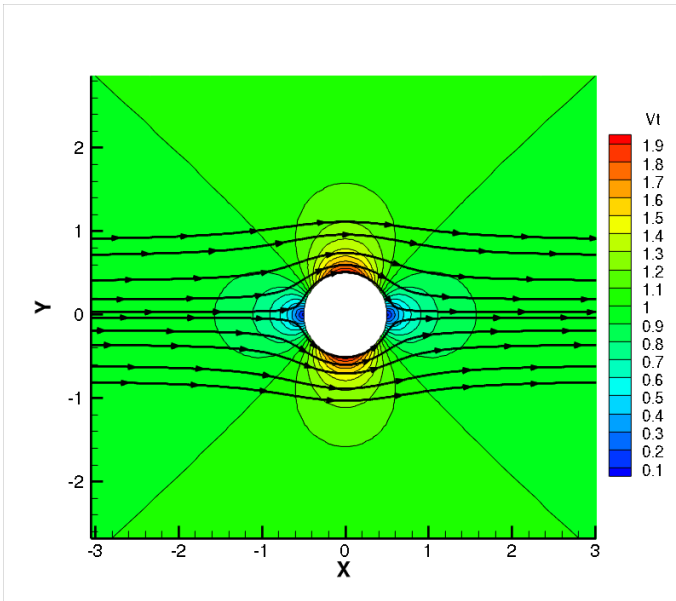

Figure 6. Stream Traces over Velocity Magnitude Contours

The streamlines clearly show what is expected from an inviscid solution. The cylinder surface is treated as a streamline, with flow clearly moving around the cylinder symmetrically.

Figure 7 shows the surface velocity magnitude around the cylinder:

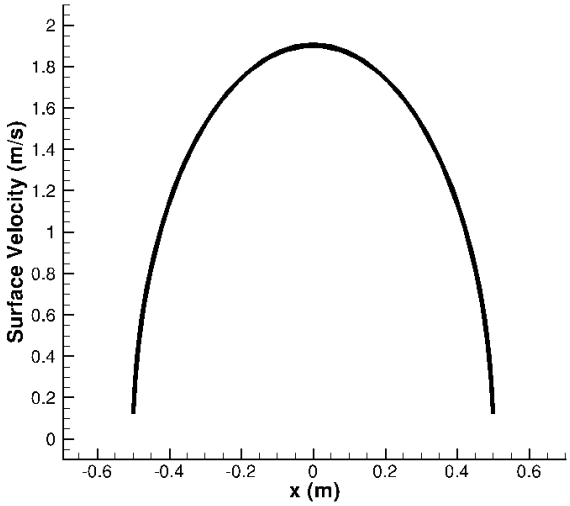

Figure 7. Cylinder Surface Velocity

This also behaves as expected, with the velocity being symmetric about the center of the cylinder.

Figure 8 shows the plot of the error versus mesh spacing for the velocity potential and the velocity magnitude:

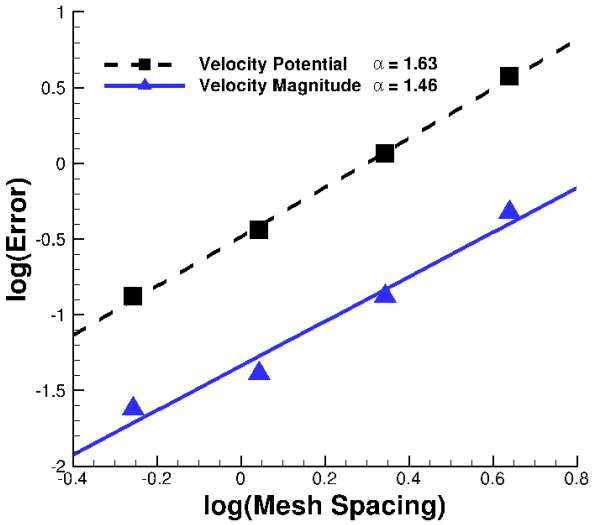

Figure 6. Velocity Potential Error (Left) and Velocity Magnitude Error (Right)

Conclusions

The finite element method clearly produces all flow features expected from an inviscid solution. The channel case provides an example similar to a Venturi tube, with the velocity at the throat being higher than at the inlet or outlet. The streamlines from this case also make it apparent that the solution correctly propagates throughout the channel, with the flow moving smoothly around the bump, all the way to the upper wall. The cylinder case clearly demonstrates the expected symmetry, with the isopotential lines being perpendicular to the surface. The streamlines for this case also verify an accurate inviscid solution, with the surface being a streamline.

Figure 6 shows that the order of accuracy of the finite element method is second order accurate in calculating the velocity potential and first order accurate in calculating the velocity magnitude, given that the slope for the potential error versus mesh spacing was approximately 2, and the slope of the velocity error versus mesh spacing is approximately 1. This implies that a reduction in average mesh spacing of 2 will result in reducing the error by a factor of four for the velocity potential and a factor of two for the velocity magnitude, which matches the observed error decline with each increasingly fine mesh.

Improvements to this code include implementing a better matrix solver than the Point Jacobi method, such as the Conjugate Gradient method or Successive Over-Relaxation. Point Jacobi is a very slow iterative method, and changing the solver will drastically improve solution time, since the solver subroutine is where the vast majority of computation time takes place.

References

Pletcher, Richard H., Dale A. Anderson, and John C. Tannehill. *Computational Fluid Mechanics and Heat Transfer*. Boca Raton, FL: CRC, 2013. Print.

"Numerical Computation of Internal and External Flows, Computational Methods for Inviscid and Viscous Flows 1st Edition." *Numerical Computation of Internal and External Flows, Computational Methods for Inviscid and Viscous Flows 1st Edition by Hirsch*. N.p., n.d. Web. 18 Feb. 2013.

"Numerical Recipes [Hardcover]." *Numerical Recipes: Amazon.co.uk: William H. Press, Saul A. Teukolsky, William T. Vetterling, Brian P. Flannery: Books*. N.p., n.d. Web. 18 Feb. 2013.